Communication

Microstructure Characterization and Battery Performance Comparison of MOF-235 and TiO$_2$-P25 Materials

Zilong Zhao [1], Xiaowei Jiang [2], Sirui Li [3], Liang Li [4], Zhiyuan Feng [1,*] and Huansheng Lai [2,*]

1   School of Chemical Engineering and Technology, Sun Yat-sen University, Zhuhai 519082, China;
    zhaozlong@mail.sysu.edu.cn
2   Sino-French Institute of Nuclear Engineering and Technology, Sun Yat-sen University, Zhuhai 519082, China;
    jiangxw8@mail2.sysu.edu.cn
3   Chemical Science Division, Lawrence Berkeley National Laboratory, Berkeley, CA 94720, USA; siruili@lbl.gov
4   School of Physics, Engineering and Computer Science, University of Hertfordshire, Hatfield AL10 9AB, UK;
    l.li30@herts.ac.uk
*   Correspondence: fengzhy25@mail.sysu.edu.cn (Z.F.); laihsh@mail.sysu.edu.cn (H.L.)

Abstract: The growing interest in energy storage has led to the urgent need for the development of high-performance cathode electrodes. The commercialized materials MOF-235 and TiO$_2$-P25 exhibit characteristics that may be suitable as electrodes but there are inherent challenges that have yet to be addressed in the literature. In this study, a high-pressure hydrothermal synthesized MOF-235 and sol-gel-made TiO$_2$-P25 were tested for battery performance. The results indicate that MOF-235 does not possess the desired performance due to uncontrollable agglomeration. On the other hand, TiO$_2$-P25 showed good cycling life, and the performance can be further optimized by doping and minimizing the particle size. Additionally, SEM and TEM were applied for surface characterization, providing evidence that mesoporous TiO$_2$-25 inhibits photo-generated carrier recombination. The mesoporous energy storage mechanism of those two materials is also discussed. This research will provide technical support for the industrialization of those two mesoporous materials.

Keywords: TiO$_2$-P25; MOF-235; nanocomposite; TEM; voltametric; microstructure characterization

1. Introduction

The growing anxieties toward the energy crisis and environmental pollution have stimulated global efforts to explore sustainable and clean energy sources to substitute fossil fuels [1–3]. Society requires levels of energy storage that exceed the limits of current technologies if we are to significantly reduce CO$_2$ emisions [4,5]. Among the various energy storage technologies, the use of electrochemical secondary batteries is a promising method for large-scale power storage because of its flexibility, high energy conversion efficiency, and simple maintenance [6]. Now, lithium-ion (Li-ion) batteries have been widely used in portable electronics and also in the emerging hybrid electric vehicles [7,8]. However, the limited lithium resources restrict its large-scale application [9]. As the demand continues to grow, it will unavoidably lead to a steady increase in cost, which will be detrimental to the widespread development of new battery systems [10]. Furthermore, TiO$_2$ has attracted significant research interest, principally due to its abundance, nontoxicity, and good stability [11,12]. However, TiO$_2$ is a wide-bandgap semiconductor, which can only absorb ultraviolet light [13]. Due to the low absorption efficiency, the catalytic effect is not obvious. Therefore, it is significant to develop a visible light-responsive photo-catalyst, and some efforts have been made to develop "second-generation" TiO$_2$ and other narrow bandgap semiconductors that can absorb visible light [14]. Metal-organic frameworks (MOFs), consisting of inorganic moieties and organic linkers, provide a large porous framework and have been found suitable for applications in water purification [15], Li-ion [16] and Na-ion batteries [17]. Such materials exhibit several benefits when employed

as electrode materials, including, (1) the working potential can be tuned to a desirable level, thereby lowering the risk of exothermic reaction with electrolyte; (2) better thermal stability and low-cost atomic separation than pure organic compounds; (3) most significantly, their special large porous frameworks with a large surface area allow for improved interfacial charge transfer, leading to potential applications in secondary-ion batteries [9,15]. Among many different types of MOF materials, Fe-MOF is the simplest and most convenient to prepare. Other Cu-MOF and Co-MOF materials are relatively complicated to prepare and have been studied by many scientists, and most of the studies are related to loaded nano semiconductor nanomaterials with good performance [18]. Therefore, Fe-MOF-235 was chosen in this research to compare its battery performance with TiO_2-P25.

In this study, MOF-235 was synthesized through a high-pressure hydrothermal method, and TiO_2-P25 was prepared using a sol-gel method. Those two different powders were then coated on titanium foil as a cathode electrode. The battery performance were tested and surface characterization were applied. The characterization results were analyzed in the framework of energy storage context. This research will provide technical support for the industrialization of those two mesoporous materials.

2. Materials and Methods

2.1. Sample Preparation

MOF-235 was prepared in a typical process. Firstly, terephthalic acid (BDC, 4.0 mmol) was dissolved in 80 ml N, N0-dimethylformamide (DMF) solution with sonication in 0.5 h. Secondly, an appropriate amount of ferric trichloride hexahydrate ($FeCl_3 \cdot 6H_2O$) and 80 mL of anhydrous ethanol was added to the solution from the previous step and stirred for 0.1 h. The previous mixed solution was transferred into a hydrothermal reactor, and it then reacted in a box-type electric furnace at 85 °C for 24 h. After cooling to room temperature, the collected precipitate was obtained by filtration and washed several times with anhydrous ethanol and DMF. Finally, after drying at 140 °C for 6 h, the final product was obtained.

Tetra-n-butylorthotitanate [Ti(O-i-C4H9) 4] (TB) which contains ≥98% Ti and ethanol absolute (EtOH) were prepared to synthesize Ti-based sol. Hydrochloric acid was added as a catalyst to increase the hydrolysis rate of the mixture. The mole ratio of the components was optimized to EtOH:TB = 50:1, with respect to the size of nanoparticle produced by the sol. Commercial TiO_2-P25 particles (average particle size = 25 nm) were dispersed into the Ti-based sol at a concentration of 0.2 g/mL for 30 min under vigorous magnetic stirring and then placed in an ultrasonic bath for 5 h. The temperature of the ultrasound bath was maintained at 80 °C. The sonicated mixture was then dried at 80 °C overnight, followed by calcination in a nitrogen-protection furnace at 500 °C for 6 h to convert the amorphous TiO_2 into anatase phase.

2.2. Performance Test and Surface Characterization

The previous step prepared MOF-235 and TiO_2-P25 were ground with a small amount of binder, respectively. Then, it was coated on a 1 mm × 20 mm × 40 mm titanium foil as a cathode electrode. The battery performance, cyclic voltammetry (CV) characteristics and storage stability, were tested on an electrochemical workstation (CS350, CorrTest, Wuhan, China). Scan rate of CV was 100 mV/s. The electrolysis cell was composed of a standard three-electrode arrangement using a Pt sheet counter electrode and a saturated Ag/AgCl reference electrode. All experiments were tested in 1M NaCl electrolyte at room temperature. Surface characterization was carried out on an XPERT-PRO X-ray diffraction (XRD) system. The microstructures were examined by using a scanning electron microscope (SEM, MIRA3, TESCAN, Czech) equipped with an Oxford electron backscattered diffraction system and a transmission electron microscope (TEM, JEOL-2100F, JEOL, Tokyo, Japan). For Brunauer-Emmett-Teller (BET) analysis, each sample was pre-dried in an oven at 150 °C in 6 h. Then, degassed overnight at 200 °C under high vacuum. The textural properties were determined by nitrogen sorption at −196 °C. The surface area was calculated by using

the BET method and the total pore volume was determined from the amount of nitrogen adsorbed. The pore-size distribution was determined by a non-local density functional theory (NLDFT) method using nitrogen-adsorption isotherms.

3. Results and Discussion

3.1. Surface Characterization via SEM and XRD

Figure 1 presents SEM images of the MOF-235 and TiO_2 mesoporous composite. The chemical formula of MOF-235 is $[Fe_3O(1,4BDC)_3(DMF)_3][FeCl_4]*(DMF)_3$, which is composed of linear organic terephthalate linking with octahedral Fe-based tripolymer. The organic and inorganic units share the joint angle, constructing a periodical reticular porous structure with a huge pore volume [9]. According to the morphology characters in Figure 1a,b, MOF-235 was successfully synthesized and well-matched with the literature [19,20]. However, Fig 1b indicates a heavy agglomeration among metal ions and organic ligands. If the separation is unable to reach the atomic level, the active center cannot be fully exposed, which affected the energy storage performance of MOF-235. Zhao et al. studied the graphene doped TiO_2 mesoporous materials for photocathode protection [21]. The graphene doped TiO_2 mesoporous materials were prepared by the sol-gel method under ultrasonic radiation. Adapted from it, the porous TiO_2 material was successfully made, which was evidenced by Figure 1c,d. A group of nanoscopic semiconductors, such as TiO_2, SnO_2, and ZnO had been used as a photocatalyst, amongst which TiO_2 was the most widely used because of its advantages such as suitable band gap for redox reactions, long-term stability, and low cost. However, as a single component semiconductor photocatalyst, TiO_2 had an inherent drawback in that the photogenerated charge carriers (hole–electron pairs) are able to recombine significantly [22]. Therefore, the preparation of mesoporous or nano-pored TiO_2 nanomaterials could reduce the recombination of photogenerated charge carriers and improve the performance of semiconductor materials.
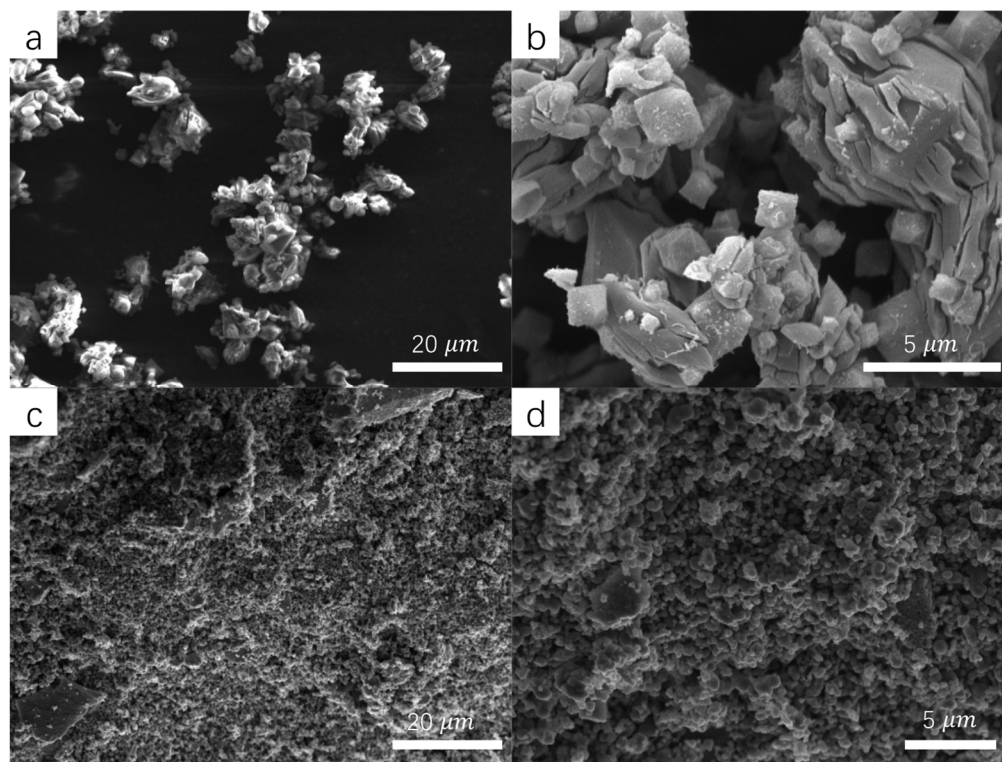

Figure 1. SEM images of the MOF-235 (**a,b**) and TiO_2-P25 mesoporous composite (**c,d**).

As shown in Figure 2, the crystal structure of the as-synthesized MOF-235 can be well matched with standard data according to the references [23]. Porous TiO_2 is a wide-

bandgap semiconductor with stable performance and a high specific surface area, which can be used as a catalyst and battery cathode [24–26]. TiO_2 is divided into the anatase phase and rutile phase. Through heat treatment, amorphous TiO_2 begins to transform into anatase at 350 °C, and the rutile phase begins to appear at 500 °C. When the temperature reaches 700 °C, the anatase phase disappears and the remaining is rutile phases. As the heat-treatment temperature continues to increase, the rutile phase particles grow larger in size [27–29]. Therefore, in this work, heat-treatments at 500 °C for 6h yielded mixed TiO_2 phases with anatase as the main phase. Figure 2 shows that the TiO_2 phase was mainly anatase phase after heat treatment. This is similar to the commercial TiO_2-P25, which has anatase phase: rutile phase = 80:20. The TiO_2 prepared in this way had high activity and the particle size was controlled at the nanometer level.
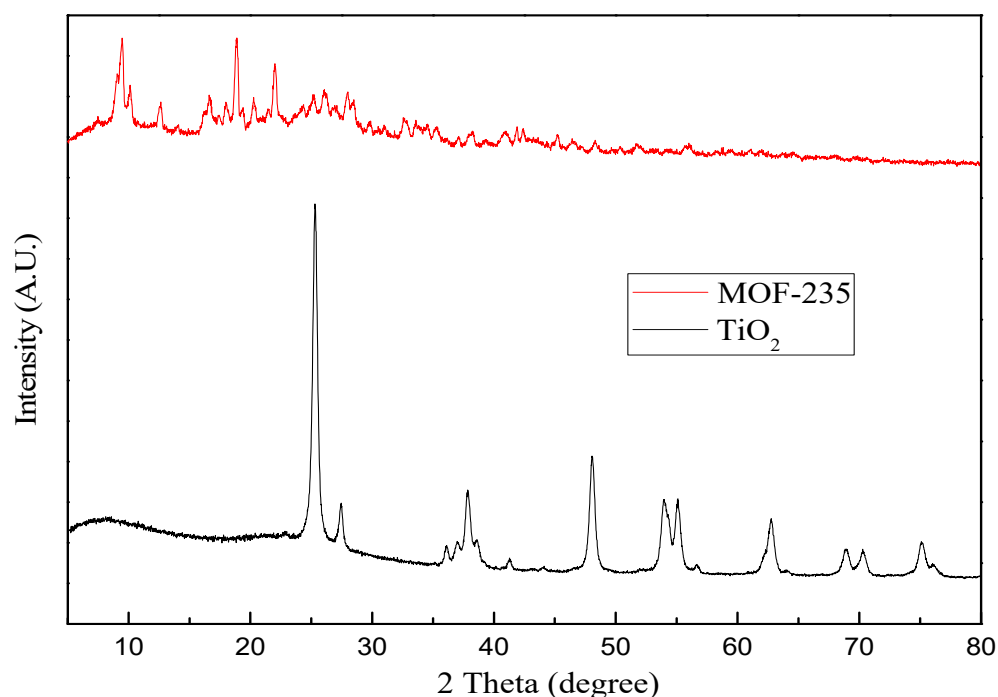

Figure 2. XRD patterns of the MOF-235 and TiO_2-P25 mesoporous composite.

3.2. Battery Performance Analysis via Cyclic Voltammetric, Charge–Discharge, and TEM Characterization

Since Gratzel et al. developed a new type of solar cell based on nanocrystalline TiO_2 electrodes, dye-sensitized solar cells (DSSCs) have attracted greater interest due to their high energy conversion efficiency and low-cost alternatives to silicon-based commercial solar cells [30–32]. Additionally, the nanocrystalline TiO_2 electrode has a high specific surface area and stability. Voltammetry is an electrochemical-analysis method based on the determination of the current-voltage curve (voltammetric curve) during electrolysis. By cyclic voltammetry, the reversibility of the electrode can be judged. If the reaction is reversible, the curve is symmetrical at the top and bottom, and if the reaction is not reversible, the curve is asymmetrical at the top and bottom [33]. Figure 3a presents a poor symmetry, while Figure 3c demonstrates good symmetry. Additionally, the cyclic voltammogram in Figure 3c shows that the ratio of the cathode peak current and anode peak current are close to 1. It indicates the high degree of reversibility of the system. Therefore, Figure 3c,d show that TiO_2 exhibits a stable energy storage cycle.
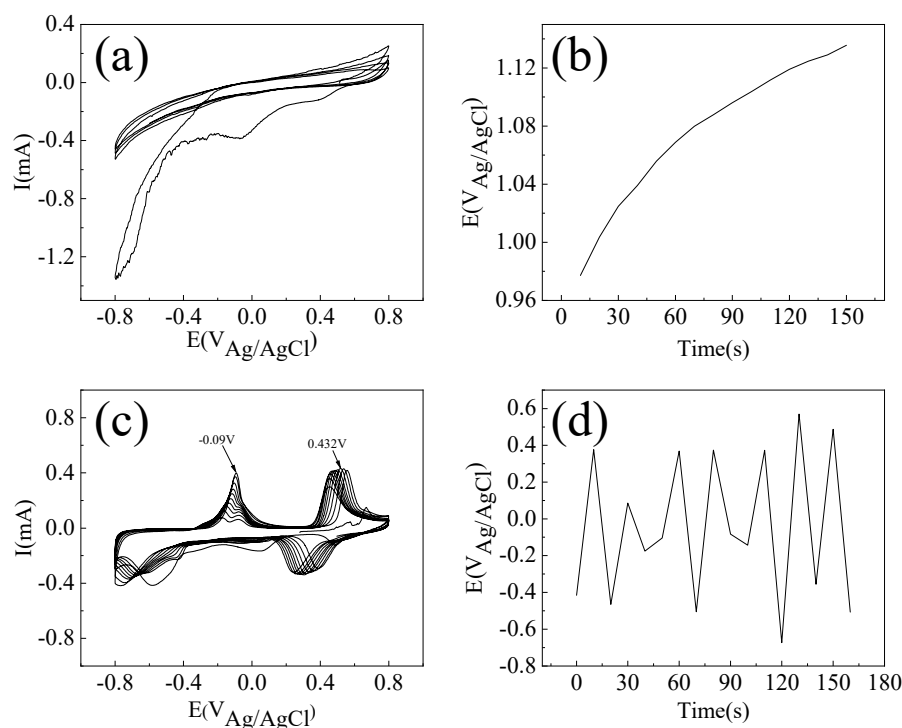
Figure 3. Cyclic-voltammetry (CV) characteristics of (**a**) MOF-235 and (**c**) TiO$_2$-P25 mesoporous composite. The charge discharge performance of (**b**) MOF-235 and (**d**) TiO$_2$-P25 mesoporous composite. All experiments were tested in 1M NaCl electrolyte at room temperature. The electrolysis cell was composed of a standard three-electrode arrangement using a Pt sheet counter electrode and a saturated Ag/AgCl reference electrode.

The low energy density and low power density could be improved by reducing the particle size, increasing the specific surface area, and doping with other elements. MOF and COF materials are also potential candidates for materials with high energy density, high power density and long-cycle stability in the field of electrochemical energy storage [7,34,35]. However, Figure 3a,b showed that MOF-235 had a low energy density and poor cycle stability, which were mainly caused by agglomeration. It needs to be combined with other high-energy storage materials to achieve the structural advantages of MOF and COF materials. Therefore, the research of electrochemical energy storage material focuses on the development of ultrafine-crystalline nanomaterials and combines the advantages of each material to prepare composite materials.

The microstructure, grain orientations, and composition distribution of crystalline materials are key to characterizing and determining various properties of materials. The lack of any kind of information makes it difficult for us to resolve the challenges of a certain material [36–39]. To this end, TEM characterization at the 5nm scale is the key to analyzing the structure of the material [40,41]. In Figure 4a,b, the TEM images indicates the mesoporous structure located in the sol-gel made TiO$_2$-P25. According to Figure 4c,d, the high-resolution image illustrates that the lab-made TiO$_2$-P25 was anatase. The mesoporous structure allowed TiO$_2$-P25 to exhibit a stable energy storage cycle and good battery performance in Figure 3c,d. As shown in Figure 5, the pore size was varied between 1–12 nm, which indicated a successful preparation of the mesoporous material. Additionally, the specific surface area of the mesoporosity TiO$_2$ materials was 28 cm^3/g. The low specific surface area was due to agglomeration. Therefore, increasing the specific surface area by reducing agglomeration was an important improvement direction to improve the cell performance of the mesoporosity TiO$_2$ materials.
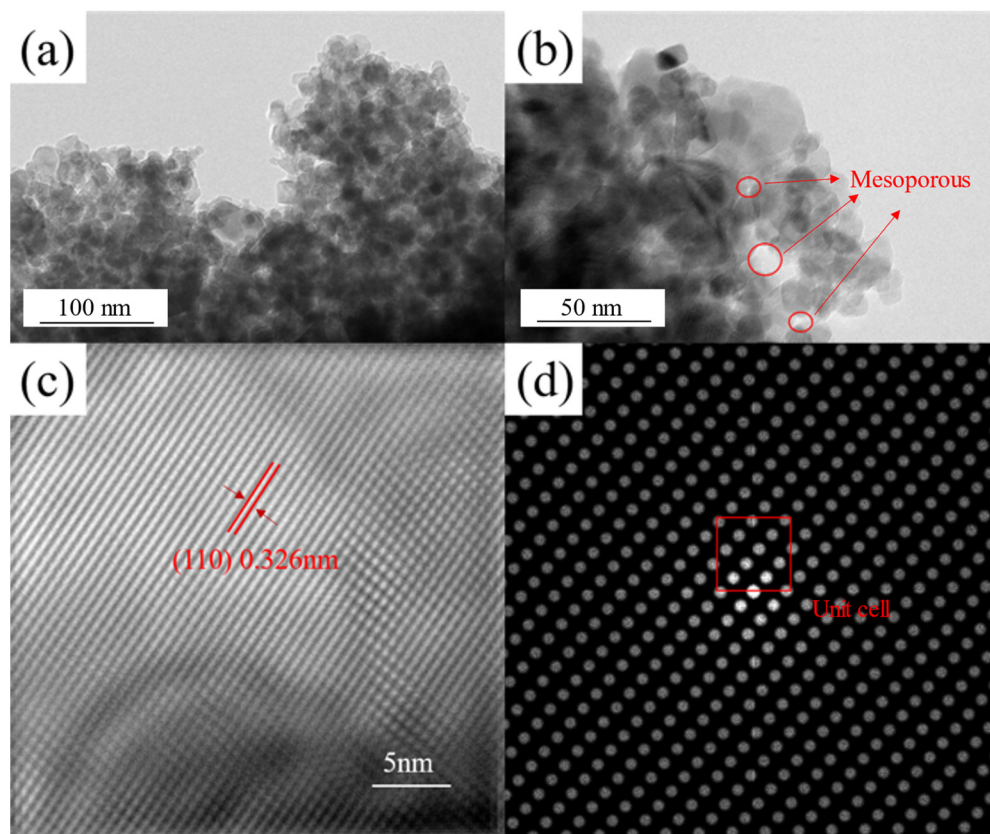
Figure 4. (**a**,**b**)TEM images of the TiO_2-P25 mesoporous composite. (**c**) High-resolution TEM image of the TiO_2-P25. (**d**) The selected area diffraction pattern from the (**c**).
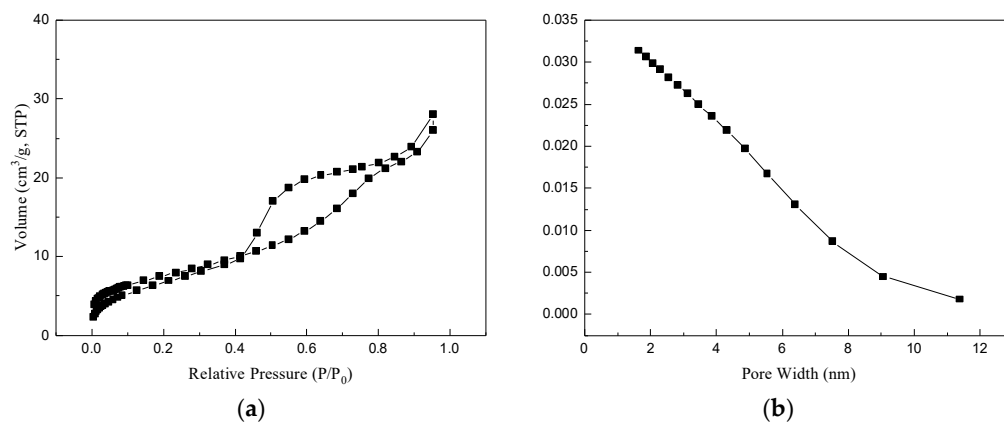

Figure 5. (**a**) BET nitrogen adsorption-desorption isotherm and (**b**) pore size distribution curve of TiO_2-P25 materials.

4. Conclusions

1. The preparation of mesoporous or nano-pored TiO_2 nanomaterials could reduce the recombination of photogenerated charge carriers and was found to have improved the performance of semiconductor materials.

2. MOF-235 had a low energy density and poor cycle stability, which were mainly caused by agglomeration. This material needs to be combined with other high-energy storage materials to achieve the structural advantages of MOF materials.

3. The development of ultrafine-crystalline nanomaterials and the preparation of composite materials by combining the advantages of each material is the main research focus in the field of electrochemical energy storage.

References

1. Nong, S.; Dong, W.; Yin, J.; Dong, B.; Lu, Y.; Yuan, X.; Wang, X.; Bu, K.; Chen, M.; Jiang, S.; et al. Well-Dispersed Ruthenium in Mesoporous Crystal TiO_2 as an Advanced Electrocatalyst for Hydrogen Evolution Reaction. *J. Am. Chem. Soc.* **2018**, *140*, 5719–5727. [CrossRef]
2. Zhang, T.; Zhou, H.S. A reversible long-life lithium-air battery in ambient air. *Nat. Commun.* **2013**, *4*, 1817. [CrossRef]
3. Jin, Y.; Liu, K.; Lang, J.L.; Zhuo, D.; Huang, Z.Y.; Wang, C.A.; Wu, H.; Cui, Y. An intermediate temperature garnet-type solid electrolyte-based molten lithium battery for grid energy storage. *Nat. Energy* **2018**, *3*, 732–738. [CrossRef]
4. Aurbach, D.; McCloskey, B.D.; Nazar, L.F.; Bruce, P.G. Advances in understanding mechanisms underpinning lithium-air batteries. *Nat. Energy* **2016**, *1*, 128. [CrossRef]
5. Pasta, M.; Wessells, C.D.; Huggins, R.A.; Cui, Y. A high-rate and long cycle life aqueous electrolyte battery for grid-scale energy storage. *Nat. Commun.* **2012**, *3*, 1149. [CrossRef]
6. Hwang, J.Y.; Myung, S.T.; Sun, Y.K. Sodium-ion batteries: Present and future. *Chem. Soc. Rev.* **2017**, *46*, 3529–3614. [CrossRef]
7. Luo, Z.; Liu, L.; Ning, J.; Lei, K.; Lu, Y.; Li, F.; Chen, J. A Microporous Covalent-Organic Framework with Abundant Accessible Carbonyl Groups for Lithium-Ion Batteries. *Angew. Chem.-Int. Ed.* **2018**, *57*, 9443–9446. [CrossRef]
8. Wang, K.L.; Jiang, K.; Chung, B.; Ouchi, T.; Burke, P.J.; Boysen, D.A.; Bradwell, D.J.; Kim, H.; Muecke, U.; Sadoway, D.R. Lithium-antimony-lead liquid metal battery for grid-level energy storage. *Nature* **2014**, *514*, 348. [CrossRef]
9. Deng, Q.; Feng, S.; Hui, P.; Chen, H.; Tian, C.; Yang, R.; Xu, Y. Exploration of low-cost microporous Fe(III)-based organic framework as anode material for potassium-ion batteries. *J. Alloys Compd.* **2020**, *830*, 154714. [CrossRef]
10. Larcher, D.; Tarascon, J.M. Towards greener and more sustainable batteries for electrical energy storage. *Nat. Chem.* **2015**, *7*, 19–29. [CrossRef]
11. Wu, T.W.; Kong, W.H.; Zhang, Y.; Xing, Z.; Zhao, J.X.; Wang, T.; Shi, X.F.; Luo, Y.L.; Sun, X.P. Greatly Enhanced Electrocatalytic N-2 Reduction on TiO_2 via V Doping. *Small Methods* **2019**, *3*, 8. [CrossRef]
12. Li, Z.H.; Luo, L.; Li, M.; Chen, W.S.; Liu, Y.G.; Yang, J.R.; Xu, S.M.; Zhou, H.; Ma, L.N.; Xu, M.; et al. Photoelectrocatalytic C-H halogenation over an oxygen vacancy-rich TiO_2 photoanode. *Nat. Commun.* **2021**, *12*, 6698. [CrossRef]
13. Ramesh, T.; Nayak, B.; Amirbahman, A.; Tripp, C.P.; Mukhopadhyay, S. Application of ultraviolet light assisted titanium dioxide photocatalysis for food safety: A review. *Innov. Food Sci. Emerg.* **2016**, *38*, 105–115. [CrossRef]
14. Tang, C.; Bai, H.; Liu, L.; Zan, X.; Gao, P.; Sun, D.D.; Yan, W. A green approach assembled multifunctional Ag/AgBr/TNF membrane for clean water production & disinfection of bacteria through utilizing visible light. *Appl. Catal. B-Environ.* **2016**, *196*, 57–67. [CrossRef]
15. Rego, R.M.; Sriram, G.; Ajeya, K.V.; Jung, H.Y.; Kurkuri, M.D.; Kigga, M. Cerium based UiO-66 MOF as a multipollutant adsorbent for universal water purification. *J. Hazard. Mater.* **2021**, *416*, 125941. [CrossRef]
16. Liu, Q.; Yu, L.; Wang, Y.; Ji, Y.; Horvat, J.; Cheng, M.-L.; Jia, X.; Wang, G. Manganese-Based Layered Coordination Polymer: Synthesis, Structural Characterization, Magnetic Property, and Electrochemical Performance in Lithium-Ion Batteries. *Inorg. Chem.* **2013**, *52*, 2817–2822. [CrossRef]
17. Dong, C.; Xu, L. Cobalt- and Cadmium-Based Metal-Organic Frameworks as High-Performance Anodes for Sodium Ion Batteries and Lithium Ion Batteries. *ACS Appl. Mater. Interfaces* **2017**, *9*, 7160–7168. [CrossRef]
18. Li, G.; Xia, L.; Dong, J.; Chen, Y.; Li, Y. 10 - Metal-organic frameworks. In *Solid-Phase Extraction*; Poole, C.F., Ed.; Elsevier: Cambridge, MA, USA, 2020; pp. 285–309.
19. Simonsson, I.; Gardhagen, P.; Andren, M.; Tam, P.L.; Abbas, Z. Experimental investigations into the irregular synthesis of iron(iii) terephthalate metal-organic frameworks MOF-235 and MIL-101. *Dalton Trans.* **2021**, *50*, 4976–4985. [CrossRef]
20. Asheghhosseini, A.; Zolgharnein, J. Iron terephthalate metal-organic framework (MOF-235) as an efficient adsorbent for removal of toluidine blue dye from aqueous solution using Box-Behnken design as multivariate optimization approach. *J. Iran. Chem. Soc.* **2020**, *17*, 2663–2673. [CrossRef]
21. Zhao, Z.; Lai, H.S.; Li, H.; Li, L. Preparation and Properties of Graphene Doped TiO_2 Mesoporous Materials for Photocathode Protection. *Int. J. Electrochem. Sci.* **2021**, *16*, 210316. [CrossRef]
22. Zhang, R.; Wu, H.; Lin, D.D.; Pan, W. Preparation of Necklace-Structured TiO_2/SnO_2 Hybrid Nanofibers and Their Photocatalytic Activity. *J. Am. Ceram. Soc.* **2009**, *92*, 2463–2466. [CrossRef]
23. Armand, M.; Grugeon, S.; Vezin, H.; Laruelle, S.; Ribiere, P.; Poizot, P.; Tarascon, J.M. Conjugated dicarboxylate anodes for Li-ion batteries. *Nat. Mater.* **2009**, *8*, 120–125. [CrossRef] [PubMed]

24. Xu, P.; Lu, J.; Xu, T.; Gao, S.; Huang, B.; Dai, Y. I-2-Hydrosol-Seeded Growth of (I-2)(n)-C-Codoped Meso/Nanoporous TiO$_2$ for Visible Light-Driven Photocatalysis. *J. Phys. Chem. C* **2010**, *114*, 9510–9517. [CrossRef]

25. Zhang, M.; Chen, W.; Xue, L.X.; Jiao, Y.; Lei, T.Y.; Chu, J.W.; Huang, J.W.; Gong, C.H.; Yan, C.Y.; Yan, Y.C.; et al. Adsorption-Catalysis Design in the Lithium-Sulfur Battery. *Adv. Energy Mater.* **2020**, *10*, 1–18. [CrossRef]

26. Zheng, J.Y.; Lyu, Y.H.; Wang, R.L.; Xie, C.; Zhou, H.J.; Jiang, S.P.; Wang, S.Y. Crystalline TiO$_2$ protective layer with graded oxygen defects for efficient and stable silicon-based photocathode. *Nat. Commun.* **2018**, *9*, 3572. [CrossRef]

27. Zhou, W.; Li, W.; Wang, J.-Q.; Qu, Y.; Yang, Y.; Xie, Y.; Zhang, K.; Wang, L.; Fu, H.; Zhao, D. Ordered Mesoporous Black TiO$_2$ as Highly Efficient Hydrogen Evolution Photocatalyst. *J. Am. Chem. Soc.* **2014**, *136*, 9280–9283. [CrossRef]

28. Zhou, W.; Sun, F.; Pan, K.; Tian, G.; Jiang, B.; Ren, Z.; Tian, C.; Fu, H. Well-Ordered Large-Pore Mesoporous Anatase TiO$_2$ with Remarkably High Thermal Stability and Improved Crystallinity: Preparation, Characterization, and Photocatalytic Performance. *Adv. Funct. Mater.* **2011**, *21*, 1922–1930. [CrossRef]

29. Wang, Y.X.; Rao, L.; Wang, P.F.; Shi, Z.Y.; Zhang, L.X. Photocatalytic activity of N-TiO$_2$/O-doped N vacancy g-C$_3$N$_4$ and the intermediates toxicity evaluation under tetracycline hydrochloride and Cr(VI) coexistence environment. *Appl. Catal. B-Environ.* **2020**, *262*, 12. [CrossRef]

30. Roy, P.; Kim, D.; Lee, K.; Spiecker, E.; Schmuki, P. TiO$_2$ nanotubes and their application in dye-sensitized solar cells. *Nanoscale* **2010**, *2*, 45–59. [CrossRef]

31. Pan, J.; Liu, G.; Lu, G.M.; Cheng, H.M. On the True Photoreactivity Order of {001}, {010}, and {101} Facets of Anatase TiO$_2$ Crystals. *Angew. Chem.-Int. Ed.* **2011**, *50*, 2133–2137. [CrossRef] [PubMed]

32. Nie, X.; Wang, J.; Duan, W.; Zhao, Z.; Li, L.; Zhang, Z. One-step preparation of C-doped TiO$_2$ nanotubes with enhanced photocatalytic activity by a water-assisted method. *Crystengcomm* **2021**, *23*, 3015–3025. [CrossRef]

33. Sandford, C.; Edwards, M.A.; Klunder, K.J.; Hickey, D.P.; Li, M.; Barman, K.; Sigman, M.S.; White, H.S.; Minteer, S.D. A synthetic chemist's guide to electroanalytical tools for studying reaction mechanisms. *Chem. Sci.* **2019**, *10*, 6404–6422. [CrossRef]

34. Jia, J.L.; Li, D.; Wan, J.F.; Yu, X.J. Characterization and mechanism analysis of graphite/C-doped TiO$_2$ composite for enhanced photocatalytic performance. *J. Ind. Eng. Chem.* **2016**, *33*, 162–169. [CrossRef]

35. Ghicov, A.; Albu, S.P.; Hahn, R.; Kim, D.; Stergiopoulos, T.; Kunze, J.; Schiller, C.A.; Falaras, P.; Schmuki, P. TiO$_2$ Nanotubes in Dye-Sensitized Solar Cells: Critical Factors for the Conversion Efficiency. *Chem. Asian J.* **2009**, *4*, 520–525. [CrossRef]

36. Xiao, Y.-X.; Ying, J.; Tian, G.; Yang, X.; Zhang, Y.-X.; Chen, J.B.; Wang, Y.; Symes, M.D.; Ozoemena, K.I.; Wu, J.; et al. Hierarchically Fractal PtPdCu Sponges and their Directed Mass- and Electron-Transfer Effects. *Nano. Lett.* **2021**, *21*, 7870–7878. [CrossRef]

37. Xiao, Y.-X.; Ying, J.; Tian, G.; Tao, Y.; Wei, H.; Fan, S.-Y.; Sun, Z.-H.; Zou, W.-J.; Hu, J.; Chang, G.-G.; et al. Highly dispersed PtPd on graphitic nanofibers and its heavy d-pi effect. *Appl. Catal. B-Environ.* **2019**, *259*, 118080. [CrossRef]

38. Huang, W.; Wang, X.; Xue, Y.; Yang, Y.; Ao, X. Hybrid nanostructures of mixed-phase TiO$_2$ for enhanced photoelectrochemical water splitting. *RSC Adv.* **2015**, *5*, 56098–56102. [CrossRef]

39. Feng, Z.Y.; Hurley, B.; Zhu, M.L.; Yang, Z.; Hwang, J.; Buchheit, R. Corrosion Inhibition of AZ31 Mg Alloy by Aqueous Selenite (SeO$_3$$^{2-}$). *J. Electrochem. Soc.* **2019**, *166*, C520–C529. [CrossRef]

40. Lee, S.S.; Bai, H.; Liu, Z.; Sun, D.D. Novel-structured electrospun TiO$_2$/CuO composite nanofibers for high efficient photocatalytic cogeneration of clean water and energy from dye wastewater. *Water Res.* **2013**, *47*, 4059–4073. [CrossRef]

41. Hwang, S.H.; Kim, C.; Jang, J. SnO$_2$ nanoparticle embedded TiO$_2$ nanofibers-Highly efficient photocatalyst for the degradation of rhodamine B. *Catal. Commun.* **2011**, *12*, 1037–1041. [CrossRef]